Experimental Mass Absorption Coefficients of Soot in Spray Combustor Flames

D. S. Babikian,* D. K. Edwards,† S. E. Karam,‡ C. P. Wood,§ and G. S. Samuelsen¶
University of California, Irvine, Irvine, California 92717

Experimental mass absorption coefficients of soot in a laboratory-scale spray combustor flame are reported for the 0.9–2.0 μm spectral range and compared to values in the literature. A specially selected JP-5 hydrocarbon fuel was sprayed through a nominal 60-deg twin-fluid nozzle at three air-to-fuel mass ratios to obtain three different soot concentrations. The measurements depended on quantitative gravimetric determination of soot concentration, gas sampling, quantitative radiometry, and optical pyrometry. Determinations of soot and gaseous species concentrations were made by traversing a water-cooled probe radially along the line of sight of the radiometer used. Optically filtered total radiometric measurements were made with selected pairs of band-pass filters. The filter bands were chosen to indicate effective gas temperature, effective soot temperature, and optical depth of soot along the radiometric line of sight. An optical pyrometer aided in confirming the soot temperature and optical depth.

Nomenclature

c = speed of light, m/s
D = diameter of soot particle, Å
f = volume fraction
h = Planck constant, J s
I = radiant intensity, W/m²sr
K = absorption coefficient, m^{-1}
k = Boltzmann constant, J/K
L = path length, m
m = mass of soot, kg
N = number of filters
n = wavelength decay exponent
q = radiant flux, W/m²
r = radius of soot particle, Å
T = temperature, K
t = optical depth
V = sample gas volume, m³
X = mole fraction
α = absorptivity
γ = ratio of absorption coefficients
δ = root-mean-square discrepancy
ϵ = emissivity
κ = mass absorption coefficient, m²/kg
λ = wavelength, m
π = 3.14159 . . .
ρ = density, kg/m³

Subscripts

a = absorption
c = computed
g = gas
m = most probable
o = reference value, observed
p = predicted
r = pyrometer
s = soot, solid
t = total
v = volume

Introduction

ONE benefit of knowing the mass absorption coefficient of soot is having the ability to assign a value of soot concentration from a flame radiation measurement. Another advantage is being able to predict flame radiation from an estimate of fuel carbon present as soot in a flame.

Mass absorption coefficient κ_a is defined as absorption coefficient K_a divided by partial density ρ_a of the absorbing mass (soot) present along a given path length L. The absorption coefficient integrated over L is the optical depth t_s

$$t_s = \int_o^L K_a \, d\ell = \int_o^L \kappa_a \rho_a \, d\ell \tag{1}$$

and the absorptivity α of the path is

$$\alpha = 1 - e^{-t_s} \tag{2}$$

Partial density ρ_a and solid volume fraction f_v are related by the solid density ρ_s

$$\rho_a = \rho_s f_v \tag{3}$$

Thus,

$$\kappa_a = K_a/\rho_a = \rho_s^{-1} (K_a/f_v) \tag{4}$$

Previously reported values of the absorption coefficient of soot have been obtained by an indirect or direct method. In the indirect method, the optical constants of soot are inferred or assumed, calculations based upon Mie scattering theory for single independent spheres are made, a particle-size distribution is measured or postulated, and the absorption coefficient is calculated. Stull and Plass[1] proceeded in this manner using the 1918 data of Senftleben and Benedict[2] for amorphous carbon and three arbitrary size distributions. Foster[3] used the same optical constants and a simplified computational procedure for small spheres as outlined by Van de Hulst.[4] Dalzell and Sarofim[5] used pressed specimens of soot gathered from

Presented as Paper 88-0539 at the AIAA 26th Aerospace Sciences Meeting, Reno, NV, Jan. 11–14, 1988; received March 17, 1988; revision received July 15, 1988.

*Research Assistant, Department of Mechanical Engineering. Student Member AIAA.
†Professor, Department of Mechanical Engineering. Fellow AIAA.
‡Research Assistant, Department of Mechanical Engineering.
§Associate Development Engineer, Department of Mechanical Engineering.
¶Professor, Department of Mechanical Engineering. Member AIAA.

real flames to obtain new values of optical constants, measured (but did not report) size distribution, and reported new calculations. Lee and Tien[6] refit the optical constants of soot and used an analytical size distribution suggested previously by Tien et al.[7] to make calculations parametric in "most probable radius" r_m.

In the direct method of determining absorption coefficient, measurements are made of transmission or emission to determine optical depth along a path of known length, and soot concentration along the path is measured by weighing a sample collected through a probe. The most extensive set of such measurements previously reported is given by Kunitomo and Sato.[8] Heavy oil was burned in one of two burners and city gas in a third burner. Spectral measurements were made from 1.8 to 5.5 μm. The probe used was described in a paper by Sato et al.[9] This water-cooled probe passed gas to a cotton filter which was weighed before and after collection. Soot deposited within the probe was "washed down, dried, and weighed." The mass absorption coefficient was then calculated from spectral measurements, the total weight of soot, and the volume of gas sample drawn.

The values of mass absorption coefficient for soot obtained by the indirect and direct methods differ considerably. For example, the city gas values reported by Kunitomo and Sato[8] at a wavelength of 1.8 μm ranged from 4000 to 4800 m^2/kg, while the value computed by Dalzell and Sarofim[5] was 2250 m^2/kg. Thus the values differ by more than a factor of two. The parametric values of Lee and Tien[6] at $\lambda = 1.8$ μm peak at a value of 3300 m^2/kg for $r_m = 1400$ Å. This value suggests that the discrepancy cannot be attributed to an optimum size of the Kunitomo and Sato city gas soot.

The present paper reports new direct values of the mass absorption coefficient for soot formed in a laboratory combustor using a JP-5 fuel spray atomized at three different nozzle air-to-fuel mass ratios (NAFR). The bandpass-filtered radiometric procedure developed previously[10] was used for the assignment of the soot optical depth, and a procedure for accurate gravimetric sampling was developed. The new results found are compared to the previously measured and calculated values.

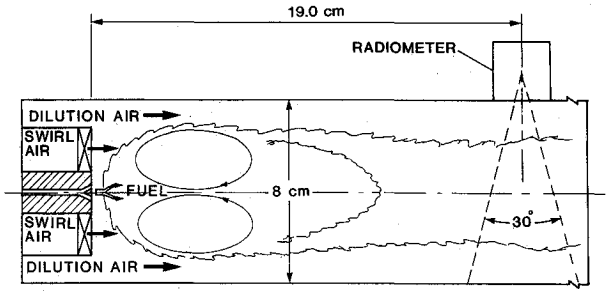

Fig. 1 Schematic of combustor.

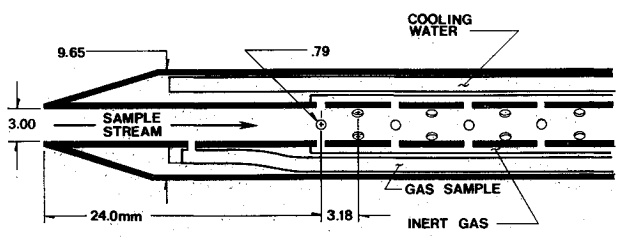

Fig. 2 Sampling probe.[12]

Apparatus and Procedure

Combustor and Fuel

Figure 1 shows the laboratory-scale combustor used for the current experiment. The combustor is described in Ref. 11. A Parker-Hannifin twin-fluid nozzle sprays a nominal 60 deg cone into dried swirl air flowing in an 80-mm-i.d. duct. Dilution air is introduced through flow straighteners in the outer annulus surrounding the swirl vanes. The swirl air enters the combustor through 60 deg swirl vanes. The dilution plus swirl air is maintained constant at 4.5×10^{-2} kg/s. An equivalence ratio of $\phi = 0.3$ is maintained constant. Air flow through the nozzle is controlled to give the desired NAFR. Three different NAFRs were selected to give a slightly sooty flame (NAFR = 3.0), a moderately sooty flame (NAFR = 2.9), and a very sooty flame (NAFR = 2.5). The range was restricted on the low soot concentration side by the need to collect a sufficient quantity of sample to allow accurate weighting, and on the high soot concentration side by the need to avoid plugging the sampling filter with soot during the course of an experiment. A JP-5 fuel with a hydrogen-to-carbon atomic ratio of 1.885 was used.

Sampling Probe

The sampling probe selected is shown in Fig. 2.[12] It is used to extract samples for both gas composition and gravimetric measurements of soot. The stainless steel probe is cooled with distilled, deionized water to preclude scaling at the high water temperatures encountered in the probe cooling jacket. The overall outside diameter of the probe is 9.65 mm, and the main sampling path has an inside diameter of 3.0 mm. The gas sample is extracted from an internal side port and piped to gas analyzers. The gas sampling procedure, the instruments used, and the assignment of mole fractions of products on a wet basis are described in Ref. 10. Figure 3 shows the mole fractions X_{H_2O}, X_{CO_2}, and X_{CO} at the different NAFRs.

The soot is extracted through the main sampling path and collected on a microquartz fiber sampling filter (Gelman). The soot sampling passage is fitted with ports for inert gas injection to dilute the mixture and to quench any reactions in the probe. The sampling filter is held in an aluminum chamber connected directly to the probe. To avoid any water vapor condensation on the filter, the aluminum chamber is kept hot by wrapping it with an electrical heating strip. An isokinetic condition at the probe inlet is maintained by regulating the suction velocity at the inlet equal to the axial velocity of the combustion gas in the combustor. Note that the gas sampling and soot sampling are conducted at two different times during a burn, so that when a soot sample is drawn no gas is extracted through the side port shown in Fig. 2.

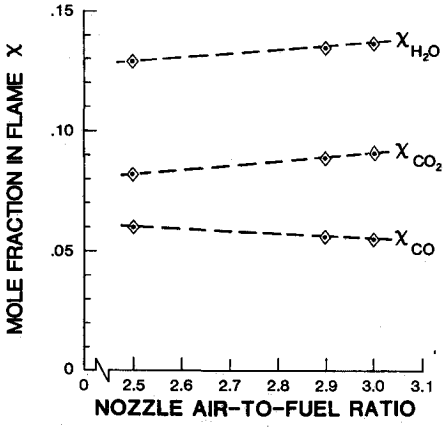

Fig. 3 Experimental values of mole fractions.

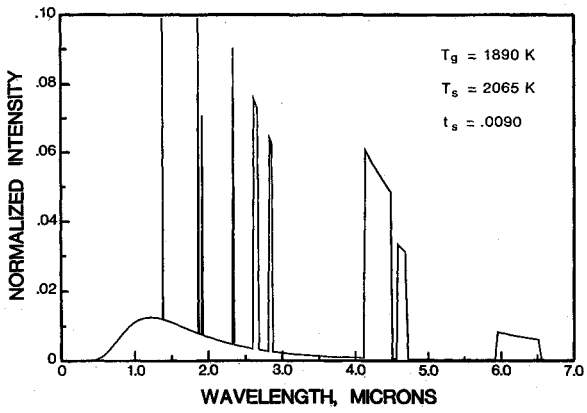

Fig. 4 Spectral layout for soot and gas bands.

Table 1 Filters and calibration constants

Filter number[a]	Transmitting spectrum,[b] μm	Calibration constants
(OCLI J + Pyrex)	1.12–1.40	0.397
F1 (LL500 + Quartz)	0.48–2.10	0.396
F2 (LL1000 + Quartz)	0.98–2.10	0.410
F3 (RS2000 + Pyrex)	1.30–1.85	0.411
F4 (RS3500 + RL1500)	1.75–3.40	0.456
F5 (58010 + RL3500)	3.60–5.00	0.598
F6 (RL3500 + Sapphire)	3.60–6.20	0.630
F7 (Sapphire + Sapphire)	0.20–6.20	0.569

[a]Filters purchased from Corion Corp., Oriel Corp., and Optical Coating Laboratory, Inc.
[b]Wavelengths shown are 50% of peak. For exact transmittance spectra, see Figs. 5 and 6.

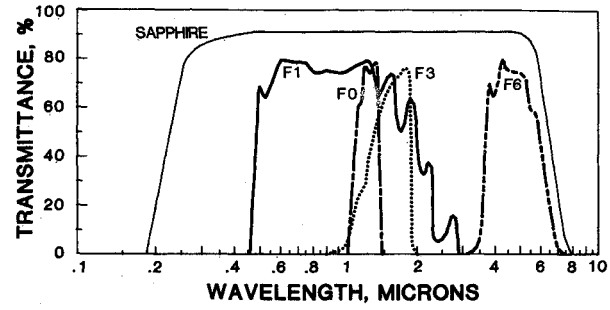

Fig. 5 Spectra of paired filters.

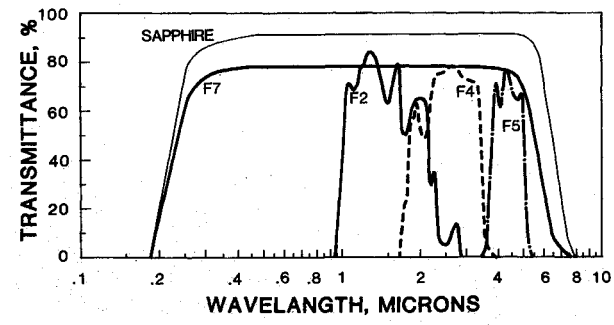

Fig. 6 Spectra of paired filters.

The sampling flow rate at the probe entrance is maintained at about 4×10^{-5} m^3/s. Inert gas (nitrogen) joins this stream along the main sampling path behind the probe entrance. To track and maintain the desired flow rates as the pressure-drop across the sampling filter increases during soot collection, the flow rates, pressures, and temperatures are recorded at each minute, and the flow rates are adjusted. In addition to the flow rates of inert and sample gas streams, the integrated volumes of the inert and sample gases are recorded minute by minute. The net flow of combustion products is obtained by subtracting the inert gas flow from the total flow.

The total soot extracted from the combustion products is the soot collected on the filter and the soot deposited on the surface of the sampling path. An electrobalance (Cahn Model 26) with an accuracy of ±0.01 mg is used to weigh the soot collected on the filter. The filter is stored in a desiccator prior to and after the soot collection to equalize any adsorbed water vapor on the filter.

The soot weight deposited on the sampling path is obtained by weighing the probe and its filter chamber before and after the experiment using an electrobalance (Mettler Model PH2000) with an accuracy of ±5 mg. In order to obtain an accurate weight for the soot deposited on the sampling path, attention is given to three important problems: 1) scaling of the probe by the deposition of solid material from the cooling water in the cooling jacket, 2) adsorption of water on the probe, and 3) the trapping of cooling water in the interior cooling jacket of the probe. To obviate the first problem, the probe was first descaled, and deionized water was then used to cool the probe during all experiments. To equalize the second and third problems, the probe was heated prior to each weighing, and dry nitrogen was blown through the water cooling jacket.

Radiometer, Filters, and Optical Pyrometer

A water-cooled and gas-purged radiometer (Medtherm Model 64P-05-24) with a nominal 15-deg half-angle field of view was used to measure the radiant flux outside the radiometer window. The term "flux" is the quantity πI, where I is averaged over the field of view. With the standard sapphire window on the detector, the radiometer responds to radiation in the 0.2 to 7.0 μm spectrum. Because of the geometrical constraints of the combustor and the radiometer rail, an annular stop was added above the sapphire window to reduce the radiometer field of view somewhat. Eleven commercial filters were selected to be used in pairs, with a 1 mm air gap spacing between the individual filters, with the goal of distinguishing the radiation from individual gas bands as well as isolating short wavelength soot radiation. Special attention was paid in selecting each filter pair to have the entire gas band of interest lie within the spectral transmittance band of that pair. Figure 4 shows the spectral locations of the gas bands and illustrates the soot emission found for the case of NAFR = 2.5.

The modified radiometer was calibrated with each pair of filters. A blackbody cavity was used for the calibration of the long wavelength filter pairs, and a high-temperature tungsten ribbon filament lamp (Optronics Laboratories, Inc., Model 550) was used for the calibration of the short wavelength filter pairs. Each filter pair transmittance spectrum was modeled with 13 spectral blocks. Details of calibration are presented in Ref. 10. Table 1 shows the filter pairs and their calibration constants, and Figs. 5 and 6 display the transmittance spectra obtained with Cary 17D and Perkin Elmer 283 spectrometers.

The radiometer, while looking at the flame through the desired filter pair, produced a signal that was monitored on the digital display of the Medtherm heat flux meter (Model H-201) and recorded on a strip chart recorder. A bright aluminum shutter was inserted between the filter pair and the flame to obtain the zero reading prior to and after each reading. The observed flux values were compared with the corresponding predicted values of a computer model (see Refs. 10, 13, and

14). An overall root-mean-square (rms) discrepancy value was calculated according to

$$\delta = \left\{ \frac{1}{N} \sum_{i=1}^{N} \left[\frac{q_p - q_o}{q_o} \right]_i^2 \right\}^{1/2} \tag{5}$$

where N is the number of filter readings considered, and q_p and q_o are the predicted and observed heat fluxes, respectively, at the detector.

Minimization of δ as explained in Ref. 10 indicates effective gas temperature T_g, soot temperature T_s, and optical depth of soot t_s. Figures 7-9 show plots of the t_s values that minimize δ for an assigned value of T_s, and the arrows on the figures mark the values of T_s where δ is minimum.

A disappearing filament optical pyrometer (Pyrometer Instrument Co., Model 95) was used to measure the apparent soot temperature T_r. The true temperature T_s is expressed as a function of optical depth t_s via emissivity ϵ_λ as follows

$$T_s = \frac{hc/\lambda k}{\ell n\{1 + \epsilon_\lambda \cdot [\exp(hc/\lambda k T_r) - 1]\}}, \quad \lambda = \lambda_r \tag{6}$$

where λ_r is taken to be 0.62 μm, and the product of the pyrometer spectral filter transmittance and the spectral response of the observer's eye is taken to be approximated by a delta function. The spectral emissivity of soot ϵ_λ is related to optical depth at λ_o by

$$\epsilon_\lambda = 1 - \exp(-t_s \cdot K_a/K_o) \tag{7}$$

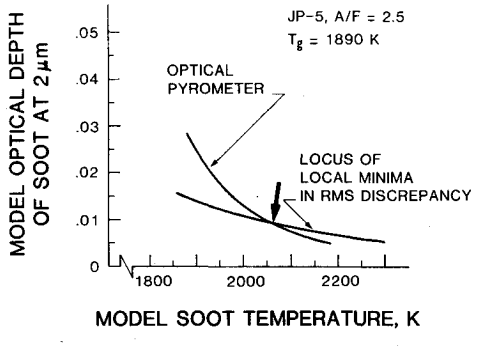

Fig. 7 Indicated optical depth of soot vs indicated soot temperature.

The ratio of K_a at $\lambda = 0.62$ μm to K_o at $\lambda_o = 2.0$ μm is denoted γ, and a value of 2.0 was assigned initially based upon the Tien and Lee dispersion model.[15] This assignment is examined more fully later in the paper.

Equation (6) is plotted in Figs. 7-9. In each figure it intersects the minimum-δ curve near the absolute minimum to confirm the assignments of t_s and T_s.

Results

Radiometric Results

The experimental readings and the computer model predictions of heat flux from the three different flames are presented in Tables 2a, 2b, and 2c. The rms discrepancies [as indicated by Eq. (5)] between the experimental values and the model predictions are within 2%. In all three flames the readings for filter F0 were disregarded because of too little soot radiation. The computer model predicts a heat flux value with filter F0 that ranges from 30 W/m^2 for the least sooty flame (NAFR = 3.0) to 110 W/m^2 for the most sooty flame (NAFR = 2.5), whereas the accuracy of the measured flux is $\pm$ 100 W/m^2 for the NAFR = 2.5 and 2.9 flames, and $\pm$ 200 W/m^2 for the case of NAFR = 3.0. For the same reasons the readings with filter F1 were excluded from the rms discrepancy assignment for the flames with NAFR = 2.9 and 3.0. Also presented in the tables are the values of effective gas temperature T_g, soot temperature T_s, and soot optical depth t_s at the minimum rms discrepancy.

Gravimetric Results

The gravimetric results shown in Table 3 were obtained by traversing the probe radially along the central line of sight of the radiometer shown in Fig. 1. For the flames with NAFR = 2.9 and 3.0 the probe was held for 2 min at each interior diametral position and 1 min at each end. The probe was moved quickly 2.54 mm between positions. The soot collecting time for the most sooty flame (NAFR = 2.5) was half of the time of the other two cases to avoid blockage of the collection filter, which would preclude the maintenance of an isokinetic sampling rate. Note that in all three cases the amount of soot deposited on the surface of the sampling path is higher, by as much as 134%, than the amount of soot collected on the soot filter. The analysis of the carbon and hydrogen content of each of the soot samples was performed by Desert Analytics. The atomic carbon to hydrogen ratios are also shown in Table 3.

Mass Absorption Coefficients

From the total mass collected and the extracted sample gas volume, and with the gas temperature and soot optical depth,

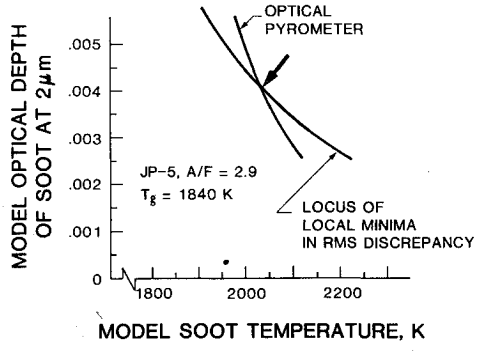

Fig. 8 Indicated optical depth of soot vs indicated soot temperature.

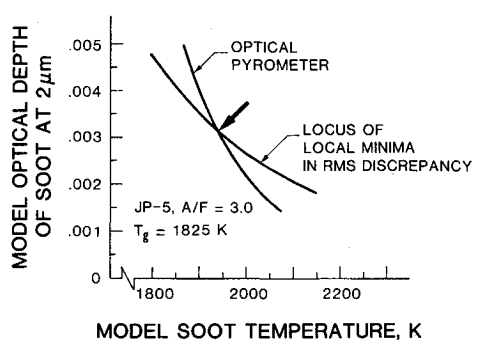

Fig. 9 Indicated optical depth of soot vs indicated soot temperature.

Table 2a Measured and predicted heat flux values for the case of NAFR = 2.5

Filter number	Experimental readings, W/m^2 q_o (±100)	Predicted values, W/m^2 q_p	Discrepancy, %
F0	—	110	—
F1	5,050	5,040	−0.2
F2	4,320	4,250	−1.6
F3	2,120	2,130	+0.5
F4	4,520	4,500	−0.4
F5	6,820	6,740	−1.2
F6	7,680	7,670	−0.1
F7	15,800	16,230	+2.6
Total spectrum	—	26,780	—
rms			1.3

Basis for predictions:
$T_g = 1890$ K $T_s = 2065$ K $t_s = 0.0090$

Optical pyrometer reading $T_r = 1520$ K

Table 2b Measured and predicted heat flux values for the case of NAFR = 2.9

Filter number	Experimental readings, W/m^2 q_o (±100)	Predicted values, W/m^2 q_p	Discrepancy, %
F0	—	50	—
F1	2,400	2,430	+1.2
F2	2,150	2,100	−2.4
F3	—	1,010	—
F4	3,250	3,290	+1.2
F5	6,560	6,470	−1.4
F6	7,400	7,340	−0.8
F7	11,950	12,260	+2.5
Total spectrum	—	20,940	—
rms			1.7

Basis for predictions:
$T_g = 1840$ K $T_s = 2040$ K $t_s = 0.0040$

Optical pyrometer reading $T_r = 1430$ K

Table 2c Measured and predicted heat flux values for the case of NAFR = 3.0

Filter number	Experimental readings, W/m^2 q_o (±200)	Predicted values, W/m^2 q_p	Discrepancy, %
F0	—	30	—
F1	1,640	1,620	−1.2
F2	1,440	1,460	+1.4
F3	—	680	—
F4	3,030	2,960	−2.4
F5	6,390	6,370	−0.3
F6	7,290	7,230	−0.8
F7	10,770	11,080	+2.8
Total spectrum	—	19,200	—
rms			1.7

Basis for predictions:
$T_g = 1825$ K $T_s = 1940$ K $t_s = 0.0032$

Optical pyrometer reading $T_r = 1360$ K

Table 3 Results of gravimetric measurements

Measurement	Nozzle air-to-fuel ratio 2.5	2.9	3.0
Collection time, min	24	48	48
Soot on filter, mg	22.31	13.17	8.67
Soot on probe, mg	30	15	10
Total soot m_t, mg	52	28	19
Gas volume V_{go},[a] m^3, $\times 10^{-5}$	3.59	4.12	4.11
Carbon/hydrogen atomic ratio	11.0	9.1	8.3

[a]At $T_o = 295$ K

the mass absorption coefficient at $\lambda = 2.0$ μm was computed according to Eq. (8)

$$\kappa_a = \frac{t_s}{\left[\frac{m_t}{V_{go}}\frac{T_o}{T_g}\right] L} \tag{8}$$

where T_o is the standard temperature at which V_{go} is computed, and L is the mean beam length viewed by the radiometer. The partial density of the absorbing mass is computed using Eq. (2).

The values of optical depth, the absorbing mass density, and the mass absorption coefficient for the three different flames are plotted vs NAFR in Fig. 10, and summarized in Table 4.

Also shown in Table 4 are the values of fuel carbon present as soot, and the soot volume fraction f_v [Eq. (3)] with the value of $\rho_s = 1560$ kg/m^3. In order to relate the soot density to the fuel carbon density it was necessary to map the axial velocity field using an argon-ion laser Doppler velocimeter and integrate to obtain a local axial mean velocity. The table shows that as the nozzle air-to-fuel ratio goes from 3.0 to 2.9 to 2.5, the volume fraction of soot present in the flame increases from 0.164×10^{-7} to 0.242×10^{-7} to 1.01×10^{-7}, respectively. These are in the ratio of 1.00 to 1.48 to 6.16, whereas the soot optical depth goes from 1.00 to 1.33 to 3.00. Accordingly, the apparent mass absorption coefficient ratio falls from 1.00 to 0.84 to 0.45.

Discussion

Experimental Uncertainties

The reported mass absorption coefficients are calculated from Eq. (8). Rearranged, Eq. (8) is

$$\kappa_a = \frac{V_{go} T_g t_s}{m_t T_o L} \tag{8a}$$

The fractional uncertainty in the calculated result is the root mean square of the fractional uncertainties of the terms. The value is influenced mainly by the large uncertainties and only a little by the small ones. These latter include the uncertainties in V_{go} and T_o, which are on the order of only 1%.

The uncertainty in the mass of soot collected is ±2.5 mg, which is 13% of the NAFR = 3.0 sample, 9% of the NAFR = 2.9 sample, and 5% of the value of NAFR = 2.5. This uncertainty is one of the major ones.

Mean beam length L comes from the ratio of the two moments of the composition profiles.[10] As shown in Table 4, it is approximately 51 mm, and is judged to be uncertain by ±4%. The value of L is input to the computer program that

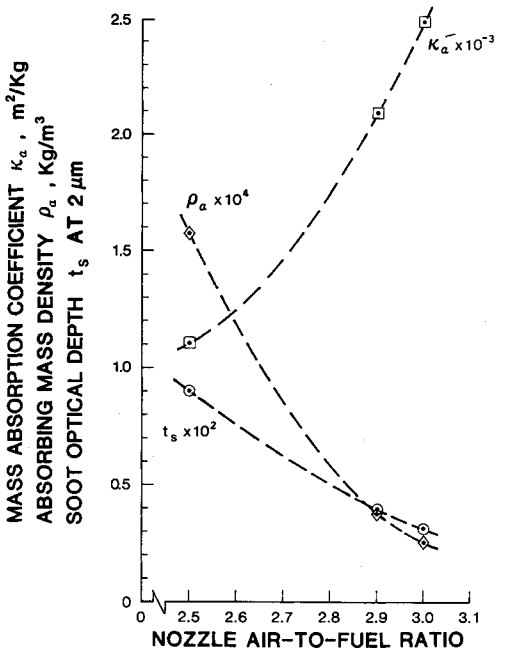

Fig. 10 Effects of nozzle air-to-fuel ratio.

Table 4 Calculated results

Calculated quantity	Nozzle air-to-fuel ratio 2.5	2.9	3.0
Path length L, m, $\times 10^{-2}$	5.13	5.06	5.05
Optical depth, t_s at $\lambda = 2.0$ μm	0.0090	0.0040	0.0032
Absorber density ρ_a, kg/m^3, $\times 10^{-5}$	15.76	3.78	2.55
Mass absorption coefficient κ_a, m^2/kg	1110	2090	2480
Fuel carbon present as soot, %	1.01	0.25	0.17
Volume fraction of soot, f_v, $\times 10^{-7}$	1.01	0.242	0.164

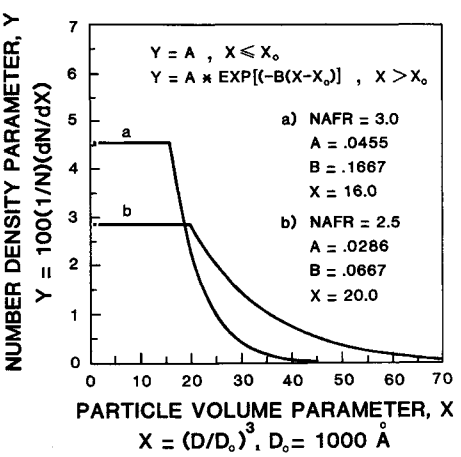

Fig. 11 Particle size distributions.

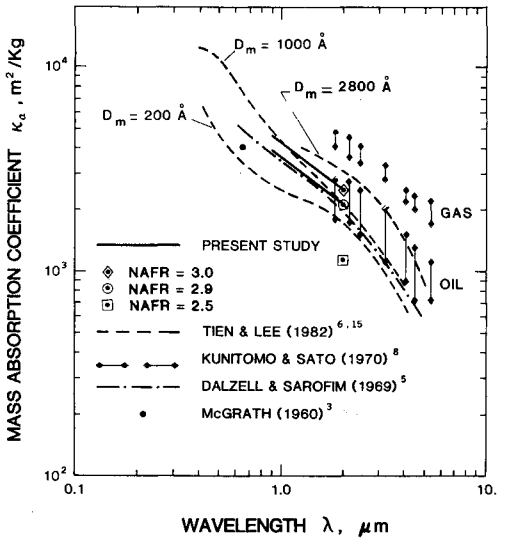

Fig. 12 Measured and calculated values of mass absorption coefficient.

assigns t_s and T_g. A variation of L by ±4% influences T_g by ∓1%, yet t_s and T_s are essentially uninfluenced. The overall uncertainty contributed by L being somewhat uncertain is thus small.

Gas temperature T_g is indicated largely by the filter F5 radiometric reading, the gas radiation model, and the gas composition. When the mole fractions of CO_2 and H_2O were varied ±10% and CO was varied ∓5% in the computer input, the indicated values of T_g, T_s, and t_s were affected by ∓1, ∓1, and ±4%, respectively. Filter F5 provided a large radiometer reading of good accuracy, and the filter pair included the entire 4.3 μm CO_2 band. The radiation from the band is highly sensitive to temperature, thus the indicated temperature is insensitive to uncertainty in radiometer signal. The same principle applies to the uncertainty in the radiation band model. Gas temperature is computed to be uncertain by ±25 K. The uncertainty in gas temperature is thus ±1.4%.

Optical depth t_s and soot temperature T_s come from radiometric readings, filter models with their calibrations, soot spectral decay exponent n, and spectral absorption ratio γ. The optical pyrometer curve, which depends on γ, agreed with the rms minima indicated by the filter model in Figs. 7–9. This observation must be tempered with the fact that for each value of n assumed, there is a value of γ that leads to agreement. For example, in addition to the pair $n = 0.8$, $\gamma = 2.0$ used here, the pairs $n = 0.9$, $\gamma = 2.3$ or $n = 1.0$, $\gamma = 2.8$ could have been used, and the indicated values of T_s and t_s for NAFR = 3.0 would have been $T_s = 1940$ K, $t_s = 0.0032$ or $T_s = 1930$ K, $t_s = 0.0030$, respectively.

The values $n = 0.8$ and $\gamma = 2.0$ are preferred because of the particle sizes found in the flames. Laser-scattering intensity-ratio data were obtained with the same combustor using the same fuel (JP-5, unpublished) and similar fuels prior to the present investigation.[16] Figure 11 shows fits to these data. Note that below $X = 1$ the data were uncertain due to experimental limitations. These data indicate that 50% of the soot mass is contained in particles larger than 2200 Å for NAFR = 3.0 and 2600 Å for NAFR = 2.5. These sizes are consistent with those observed by Scanning Electron Microscope analysis of extracted samples.[11] For 2200 to 2600 Å sizes, the calculations of Lee and Tien[6] show $n = 0.8$ and $\gamma = 2.0$ are appropriate. All factors considered, we regard our values of t_s subject to a 7% uncertainty for NAFR = 3.0.

The preceding values of uncertainty combine to give a total uncertainty of ±15% for NAFR = 3.0, ±11% for NAFR = 2.9, and ±8% for NAFR = 2.5. To these estimated

uncertainties must be added a major caveat. The soot collected by the probe may not all be at the hot temperature T_s. If some is colder, then the indicated value of m_t is too large, and the indicated mass absorption is too small. This possibility is discussed further below.

Comparisons with Others

Kunitomo and Sato[8] reported infrared emission spectrometer measurements. Their measurements are plotted in Fig. 12. Soot produced by a gas burner gave indicated values of mass absorption coefficient at 2.0 μm from 3800 to 4600 m^2/kg. Soot produced by an oil burner gave values from 1800 to 2800 m^2/kg. Qualitatively, their results showed a large range of values, depending upon the combustion conditions, and are similar to the present results. Quantitatively, the ratio of the previously reported maximum to minimum value is 4600/1800 = 2.6. The present results range from 1110 (NAFR = 2.5) to 2480 (NAFR = 3.0), giving a ratio of 2.2. However, their results are higher by 60% to 90%. One reason for the discrepancy could be experimental gravimetry. Sato et al.[9] report using solvent extraction to collect the soot deposited on the probe. Our experience is that solvent did not remove all of the deposits. We had to use repeated mechanical roddings, solvent washings, and air blasts to clean the probe after use. In view of our experience of collecting as much as half the soot specimen on the probe, we fear that their results may be overstated by as much as a factor of two.

The present results compare reasonably well with the calculations of Dalzell and Sarofim,[5] also shown in Fig. 12. Their curve passes 7% below the present measurement for NAFR = 2.9, and 21% below that for NAFR = 3.0. The calculated results of Lee and Tien for 200 and 1000 Å spheres are 1700 and 2150 m^2/kg, respectively. The latter curve passes just above the present result for NAFR = 2.9 of 2090 m^2/kg. Note that as soot diameter increases from small sizes (200 Å or less), the mass absorption coefficient rises to a maximum and then decreases because of an interference coupling in the optics. Lee and Tien's calculations for postulated size distributions show a maximum value of 3150 m^2/kg at 2.0 μm, when the most probable sphere diameter is approximately 2800 Å. This value is 27% above the experimental value obtained here for NAFR = 3.0.

Also shown in Fig. 12 is a point attributed to McGrath by Foster[3] at $\lambda = 0.65$ μm. This value can be indirectly compared to the present results by multiplying the present results at $\lambda = 2.0$ μm by $\gamma = 2.0$. Thus the present results of 2090 and 2480 for NAFR = 2.9 and 3.0, respectively, translate to 4180 and 4960 compared to McGrath's value of 4050 m^2/kg.

To summarize, the results of Kunitomo and Sato lie 90% higher than the present results, and errors in gravimetry are believed responsible for the large discrepancy. The results of Dalzell and Sarofim lie 21% below the present results for NAFR = 3.0, and the maximum calculated value of Tien and Lee lies 27% above.

Effect of NAFR

As nozzle air-to-fuel mass ratio decreases from 3.0 to 2.5, the fuel carbon converted to soot rises by a factor of six (see Table 4). The radiation measured with filter pair F1 rises by a factor of three (see Tables 2a-2c). Thus the apparent mass absorption falls by a factor of two (from 2480 to 1110 m^2/kg precisely).

A major question in interpreting the present results is why the emitted radiation grows by only a factor of three as the amount of soot grows by a factor of six. Similar behavior is seen in Kunitomo and Sato's work.[8]

A decrease in NAFR reduces the injection momentum of the liquid droplets, and a modest growth in fuel droplet size occurs with decreasing NAFR.[16] The net result is a collapse of the fuel to the center core of the combustor with an attendent increase in soot.[17] In contrast, a high droplet momentum created by a larger NAFR and a small droplet size favor the creation of less soot under the specific conditions at which the current combustor was operated. As has been stated here, the soot particle size characterizing the 50% mass fraction boundary appeared to rise from 2200 to 2600 Å as NAFR dropped from 3.0 to 2.5. According to the calculations of Lee and Tien,[6] this mild increase in soot particle size should cause an *increase* in κ_a by a few percent, not the decrease seen from 2480 to 1110 m^2/kg. Accordingly, it is suggested that at low NAFR, there are present in the radiometer field relatively cold soot particles, perhaps associated with fuel droplets in regions of insufficient combustion air, and that these colder soot particles contributed to the six-fold increase in gravimetric soot but not to the radiant emission. Thus, it is hypothesized that hot soot increased three times proportionally with the radiation, but that a new component of cold soot grew as NAFR fell from 3.0 to 2.5, and doubled the total gravimetric soot present.

Summary

Although the amount of fuel carbon converted into soot, the size spectrum of the soot particles, and the proportions of hot soot and cold soot present in a flame cannot yet be predicted from first principles, the present work does indicate the orders of magnitude of these quantities that can be expected in a spray-atomized liquid-fueled flame. The radiometric technique developed using simple, rugged, low-cost total radiometers with inexpensive filters has merit for indicating the amount of hot soot present in a flame. The gravimetric technique developed involving cooling jacket scale control and sample probe weighing is recommended. The results for mass absorption coefficient of soot reported here are independent of optical constant measurements and Mie absorption calculations and fall about midway between such calculations made by Dalzell and Sarofim[5] on the one hand, and Lee and Tien[6] on the other.

Acknowledgments

The authors acknowledge the Naval Air Propulsion Center (Navy Contract N00014-C-9151) for their support of the early stages of the work. Yasushi Sakurai's help in obtaining an English translation of Ref. 9, and Julius Glater's advice on scale removal and control are also acknowledged.

References

[1]Stull, V. R. and Plass, G. N., "Emissivity of Dispersed Particles," *Journal of the Optical Society of America*, Vol. 50, No. 2, 1960, pp. 121-129.

[2]Senftleben, H. and Benedict, E., "Über die Optischen Konstanten und die Stahlungsgesetze der Kohle," *Annalen der Physik*, Vol. 54, 1918, pp. 65-78.

[3]Foster, P. J., "Calculation of the Optical Properties of Dispersed Phases," *Combustion and Flame*, Vol. 7, 1963, 277-282.

[4]Van de Hulst, H. C., *Light Scattering by Small Particles*, Wiley, New York, 1957, pp. 119-128.

[5]Dalzell, W. H. and Sarofim, A. F., "Optical Constants of Soot and Their Applications to Heat Flux Calculations," *Journal of Heat Transfer*, Vol. 91, No. 1, 1969, pp. 100-104.

[6]Lee, S. C. and Tien, C. L., "Optical Constants of Soot in Hydrocarbon Flames," *Eighteenth Symposium (International) on Combustion*, 1981, pp. 1159-1166.

[7]Tien, C. L., Doornink, D. G., and Rafferty, D. A., "Attenuation of Visible Radiation by Carbon Smokes," *Combustion Science and Technology*, Vol. 6, 1972, pp. 55-59.

[8]Kunitomo, T. and Sato, T., "Experimental and Theoretical Study in the Infrared Emission of Soot Particles in Luminous Flame," *Heat Transfer 1970, Presented at the Fourth International Heat Transfer Conference*, Vol. III, Paris, 1970, R1.6.

[9]Sato, T., Kunitomo, T., Nakashima, F., and Fujii, H., "Study on Radiation from Luminous Flame," *Bulletin of JSME*, Vol. 9, 1966, pp. 786-777.

[10]Babikian, D. S. and Edwards, D. K., "Comparison of Experimental and Computational Values of Flame Radiation," *Journal of Thermophysics and Heat Transfer*, Vol. 2, No. 2, 1988, pp. 131-137.

[11]Wood, C. P., Smith, R. A., and Samuelsen, G. S., "Spatially-Resolved Measurements of Soot Size and Population in a Swirl-Stabilized Combustor," *Twentieth Symposium (International) on Combustion*, The Combustion Institute, 1984, pp. 1083–1094.

[12]Himes, R. M., Hack, R. L., and Samuelsen, G. S., "Chemical and Physical Properties of Soot as a Function of Fuel Molecular Structure in a Swirl-Stabilized Combustor," *Journal of Engineering for Gas Turbines and Power*, Vol. 106, 1984, pp. 103–108.

[13]Edwards, D. K., "Molecular Gas Band Radiation," *Advances in Heat and Mass Transfer*, Vol. 12, Academic, Orlando, FL, 1976, pp. 115–193.

[14]Edwards, D. K., *Radiation Heat Transfer Notes*, Hemisphere, New York, 1981, pp. 195–238.

[15]Tien, C. L. and Lee, S. C., "Flame Radiation," *Progress in Energy Combustion Science*, Vol. 8, No. , 1982, pp. 41–59.

[16]Wood, C. L. and Samuelsen, G. S., "Optical Measurements of Soot Size and Number Density in a Spray-Atomized, Swirl-Stabilized Combustor," *ASME Journal of Engineering for Gas Turbine and Power*, Vol. 107, 1985, pp. 38–47.

[17]Jackson, T. A., "Spatial Characterization of Droplet Size and Droplet Velocity in a Liquid Atomized Spray," Ph.D. Thesis, Univ. of California, Irvine, 1985.